

# SCIENTIFIC REPORTS



OPEN

## Dual-FRET imaging of IP<sub>3</sub> and Ca<sup>2+</sup> revealed Ca<sup>2+</sup>-induced IP<sub>3</sub> production maintains long lasting Ca<sup>2+</sup> oscillations in fertilized mouse eggs

Toru Matsu-ura<sup>1</sup>, Hideki Shirakawa<sup>2</sup>, Kenichi G. N. Suzuki<sup>3</sup>, Akitoshi Miyamoto<sup>1,4</sup>, Kotomi Sugiura<sup>5</sup>, Takayuki Michikawa<sup>6</sup>, Akihiro Kusumi<sup>7</sup> & Katsuhiko Mikoshiba<sup>1,8,9</sup>

In most species, fertilization induces Ca<sup>2+</sup> transients in the egg. In mammals, the Ca<sup>2+</sup> rises are triggered by phospholipase C $\zeta$  (PLC $\zeta$ ) released from the sperm; IP<sub>3</sub> generated by PLC $\zeta$  induces Ca<sup>2+</sup> release from the intracellular Ca<sup>2+</sup> store through IP<sub>3</sub> receptor, termed IP<sub>3</sub>-induced Ca<sup>2+</sup> release. Here, we developed new fluorescent IP<sub>3</sub> sensors (IRIS-2s) with the wider dynamic range and higher sensitivity (K<sub>d</sub> = 0.047–1.7  $\mu$ M) than that we developed previously. IRIS-2s employed green fluorescent protein and Halo-protein conjugated with the tetramethylrhodamine ligand as fluorescence resonance energy transfer (FRET) donor and acceptor, respectively. For simultaneous imaging of Ca<sup>2+</sup> and IP<sub>3</sub>, using IRIS-2s as the IP<sub>3</sub> sensor, we developed a new single fluorophore Ca<sup>2+</sup> sensor protein, DY3.60. With IRIS-2s and DY3.60, we found that, right after fertilization, IP<sub>3</sub> concentration ([IP<sub>3</sub>]) starts to increase before the onset of the first Ca<sup>2+</sup> wave. [IP<sub>3</sub>] stayed at the elevated level with small peaks followed after Ca<sup>2+</sup> spikes through Ca<sup>2+</sup> oscillations. We detected delays in the peak of [IP<sub>3</sub>] compared to the peak of each Ca<sup>2+</sup> spike, suggesting that Ca<sup>2+</sup>-induced regenerative IP<sub>3</sub> production through PLC produces small [IP<sub>3</sub>] rises to maintain [IP<sub>3</sub>] over the basal level, which results in long lasting Ca<sup>2+</sup> oscillations in fertilized eggs.

In most species, rises in cytosolic Ca<sup>2+</sup> concentration ([Ca<sup>2+</sup>]) trigger the egg-embryo transition. Unfertilized eggs, which are arrested at different stages of meiosis in different species, are “activated” and released from the arrest by fertilization<sup>1,2</sup>. In mammals, egg activation is triggered by a periodic series of Ca<sup>2+</sup> transients, known as Ca<sup>2+</sup> oscillations<sup>3,4</sup>. The response in mammalian eggs lasts for several hours and involves relatively low frequency, large amplitude Ca<sup>2+</sup> increases<sup>5</sup>. The multiple increases in [Ca<sup>2+</sup>] are essential for completion of all the events of egg activation in mammals<sup>5,6</sup>.

The first Ca<sup>2+</sup> transient occurs some minutes after sperm-egg fusion<sup>7</sup>. The Ca<sup>2+</sup> oscillations in mammalian eggs appear to be a result of Ca<sup>2+</sup> release via the inositol 1,4,5-trisphosphate (IP<sub>3</sub>) receptor/Ca<sup>2+</sup> release channel (IP<sub>3</sub>R) located on the intracellular Ca<sup>2+</sup> stores<sup>8</sup>. A sperm-specific phospholipase C $\zeta$  (PLC $\zeta$ )<sup>9</sup>, which produces IP<sub>3</sub> via hydrolysis of phosphatidyl 4,5-bisphosphate (PIP<sub>2</sub>), is reported as an egg-activating sperm factor<sup>10</sup> in

<sup>1</sup>Laboratory for Developmental Neurobiology, Center for Brain Sciences, RIKEN, 2-1 Hirosawa, Wako, Saitama, 351-0198, Japan. <sup>2</sup>Department of Applied Physics and Chemistry, The University of Electro-Communications, Tokyo, 182-8585, Japan. <sup>3</sup>Center for Highly Advanced Integration of Nano and Life Sciences (G-CHAIN), Gifu University, 1-1 Yanagido, Gifu, 501-1193, Japan. <sup>4</sup>Laboratory of Single-Molecule Cell Biology, Kyoto University Graduate School of Biostudies, Konoe-cho, Sakyo-ku, Kyoto, 606-8501, Japan. <sup>5</sup>Division of Mucosal Vaccines, International Research and Development Center for Mucosal Vaccine, The Institute of Medical Science, University of Tokyo, 4-6-1 Shirokanedai, Minato-ku, Tokyo, 108-8639, Japan. <sup>6</sup>Laboratory for Biotechnological Optics Research, Center for Advanced Photonics, RIKEN, 2-1 Hirosawa, Wako, Saitama, 351-0198, Japan. <sup>7</sup>Okinawa Institute of Science and Technology Graduate University, 1919-1 Tancha, Onna, Okinawa, 904-0495, Japan. <sup>8</sup>Department of Pharmacology, Keio University School of Medicine, 35 Shinanomachi, Shinjuku-ku, Tokyo, 160-8582, Japan. <sup>9</sup>Shanghai Institute for Advanced Immunochemical Studies, ShanghaiTech University, Shanghai, 201210, China. Correspondence and requests for materials should be addressed to K.M. (email: [mikosiba@brain.riken.jp](mailto:mikosiba@brain.riken.jp))

mammalian species. The microinjection of complementary RNA (cRNA) encoding PLC $\zeta$ <sup>11</sup> or recombinant PLC $\zeta$  proteins<sup>12</sup> into unfertilized mouse eggs triggers characteristic Ca<sup>2+</sup> oscillations like those observed at fertilization. Sperm from transgenic mice with significantly reduced expression of PLC $\zeta$  display a premature termination of Ca<sup>2+</sup> oscillations following *in vitro* fertilization<sup>13</sup>. PLC $\zeta$  shows extremely high Ca<sup>2+</sup> sensitivity for its enzymatic activity compared with other PLC isoforms, with 70% maximal activity at 100 nM Ca<sup>2+</sup><sup>12</sup>. Therefore, it has been considered that basal cytosolic Ca<sup>2+</sup> in the fertilized egg can stimulate PLC $\zeta$  to produce an amount of IP<sub>3</sub> sufficient to trigger the initial release of Ca<sup>2+</sup>, which has not been confirmed experimentally, since single cell imaging using fluorescent IP<sub>3</sub> indicators, such as green fluorescent protein (GFP)-fused to pleckstrin homology domain (GFP-PHD)<sup>14</sup> and fretino-2<sup>15</sup>, failed to clearly detect IP<sub>3</sub> concentration ([IP<sub>3</sub>]) changes evoked in fertilized mouse eggs<sup>16,17</sup>.

Because all PLC isoforms including PLC $\zeta$  are activated by Ca<sup>2+</sup><sup>12,18–20</sup>, there will be further increase in IP<sub>3</sub> production when [Ca<sup>2+</sup>] start to increase. This positive feedback has been proposed to play a central role for the generation of the upstroke of Ca<sup>2+</sup> transients<sup>21,22</sup>. Except for PLC $\zeta$ , members of each of the PLC families are expressed in eggs, and PLC $\beta$ 1 is reported to contribute generation of Ca<sup>2+</sup> transients<sup>23</sup> and in theory any of these could be involved in modulating Ca<sup>2+</sup> oscillations. On the other hand, the positive feedback regulation of Ca<sup>2+</sup> acting directly on the IP<sub>3</sub>R has been proposed to drive regenerative Ca<sup>2+</sup> increases<sup>24</sup>. Simultaneous detection of [Ca<sup>2+</sup>] and [IP<sub>3</sub>] is necessary to figure out the contributions of Ca<sup>2+</sup>-induced IP<sub>3</sub> production from PLCs and Ca<sup>2+</sup> release from IP<sub>3</sub>R for the generation of fertilization-induced Ca<sup>2+</sup> transients.

In the present study, we developed novel fluorescent resonant energy transfer (FRET)-based IP<sub>3</sub> sensor proteins, designated as IRIS-2s, to visualize IP<sub>3</sub> dynamics in fertilized mouse eggs. The novel IP<sub>3</sub> sensors possess an improved dynamic range compared with the previous sensor, IRIS-1<sup>25</sup>. A high IP<sub>3</sub> binding affinity variant, IRIS-2.3, can be successfully used to monitor [IP<sub>3</sub>] changes naturally induced in fertilized mouse eggs. IRIS-2s contain enhanced green fluorescent protein (EGFP) and Halo-protein with tetramethylrhodamine (TMR) ligand as FRET donor and acceptor, respectively. To monitor [Ca<sup>2+</sup>] and [IP<sub>3</sub>] changes simultaneously, we also developed a new Ca<sup>2+</sup> sensor protein, designated as DY3.60, which has enhanced cyan fluorescent protein (ECFP) as a solo fluorophore. The pair of IRIS-2s and DY3.60 contains a new set of fluorophores for dual-FRET imaging, and real time monitoring with IRIS-2s and DY3.60 provide us insights into the mechanism underlying the generation of Ca<sup>2+</sup> oscillations in mouse fertilized eggs.

## Results

**Construction of IRIS-2s.** We constructed novel IP<sub>3</sub> sensors composed of HaloTag protein (Promega), IP<sub>3</sub> binding domain (IP<sub>3</sub>BD) of mouse IP<sub>3</sub>R1<sup>25</sup>, and mEGFP (upper panel in Fig. 1a). HaloTag protein is an engineered, catalytically inactive derivative of a hydrolase that forms a covalent bond with commercially available HaloTag ligands. We used HaloTag<sup>®</sup> tetramethylrhodamine (TMR) ligand (Promega) as a FRET acceptor for mEGFP. Amino acid residues 224–575 and 224–579 of mouse IP<sub>3</sub>R1 were used for IRIS-2 and IRIS-2.3, respectively (upper panel in Fig. 1b), to manipulate the IP<sub>3</sub> binding affinity of the sensors. We constructed IRIS-2-Dmut, in which two critical amino acid residues (Thr267 and Lys508) for IP<sub>3</sub> binding have been replaced in IRIS-2, as a negative control<sup>25</sup> (upper panel in Fig. 1b). The upper panel in Fig. 1c shows emission spectrum of IRIS-2 when excited at 480 nm. Purified IRIS-2 with addition of HaloTag TMR ligand (IRIS-2<sub>TMR</sub>) showed greater TMR emission (565 nm) and lesser EGFP emission (510 nm) (green line in Fig. 1c) compared with those of untreated IRIS-2 (red line in Fig. 1c), indicating that FRET between EGFP and TMR occurs in IRIS-2<sub>TMR</sub>. The addition of 100  $\mu$ M IP<sub>3</sub> increased the EGFP emission and decreased the TMR emission (blue line in Fig. 1c), indicating that the FRET efficiency of IRIS-2<sub>TMR</sub> decreases upon IP<sub>3</sub> binding (Fig. 1a). The relative change in the EGFP/TMR emission ratio of IRIS-2<sub>TMR</sub> monitored with zero and 100  $\mu$ M IP<sub>3</sub> ( $155 \pm 26\%$ ;  $n = 3$ ) was three times larger than that of IRIS-1 ( $55.2 \pm 2.7\%$ ;  $n = 3$ ) (Fig. 1c and Supplementary Fig. 1). The high dynamic range achieved in IRIS-2 was preserved in IRIS-2.3 treated with HaloTag TMR ligand (IRIS-2.3<sub>TMR</sub>) ( $117 \pm 3\%$ ;  $n = 3$ ). Figure 1d shows the IP<sub>3</sub> dependence of the emission ratio of IRIS-2<sub>TMR</sub> and IRIS-2.3<sub>TMR</sub>. The K<sub>d</sub> value of IRIS-2.3<sub>TMR</sub> ( $0.047 \pm 0.006 \mu$ M;  $n = 3$ ; Fig. 1d) was 36-times smaller than that of IRIS-2<sub>TMR</sub> ( $1.7 \pm 0.2 \mu$ M;  $n = 3$ ; Fig. 1d). The K<sub>d</sub> value of IRIS-2<sub>TMR</sub> was 3-times larger than that of IRIS-1 ( $0.55 \pm 0.06 \mu$ M)<sup>25</sup>.

As a partner of IRIS-2s, we developed a FRET based Ca<sup>2+</sup> indicator with single fluorophore to avoid fluorescent overlapping with IRIS-2s. We introduced a non-fluorescent mutation (Y145W<sup>26</sup>) into a yellow fluorescent protein, cp173Venus, of YC3.60<sup>27</sup> (lower panels in Fig. 1a,b). The resultant protein have a fluorescent spectrum as same as ECFP, and addition of 100  $\mu$ M Ca<sup>2+</sup> decreased its emission by FRET quenching. The peak fluorescent amplitude was  $71 \pm 3\%$  ( $n = 3$ ) reduced after addition of Ca<sup>2+</sup> in DY3.60 (lower panel in Fig. 1c). Fluorescence from the three fluorophores used in IRIS-2s and DY3.60 can be easily separated (Fig. 1e). Figure 1f shows time course changes of fluorescence from DY3.60 and IRIS-2 in glutamate stimulated mGluR5-expressing HeLa cells. Less overlaps of excitation and emission spectra of IRIS-2 and DY3.60 allowed dual-FRET imaging of Ca<sup>2+</sup> and IP<sub>3</sub> even without spectral unmixing<sup>28</sup> (Fig. 1f).

**Characterization of IRIS-2s and DY3.60 expressed in cultured mammalian cells.** IRIS-2<sub>TMR</sub> and DY3.60 were uniformly distributed within the cytosol when expressed in HeLa cells (Fig. 2a–e). Halo-TMR staining increased fluorescent signal detected by a 573–613-nm emission filter (Fig. 2b,d). The frequency of Ca<sup>2+</sup> oscillations monitored with Indo-5F in mGluR5-expressing HeLa cells stimulated with 10  $\mu$ M glutamate were not significantly different among IRIS-2-, IRIS-2-Dmut-, and DY3.60-expressing cells ( $50 \pm 16$  mHz for IRIS-2,  $n = 9$ ;  $55 \pm 6$  mHz for IRIS-2-Dmut,  $n = 4$ ;  $47 \pm 10$  mHz,  $n = 6$  for DY3.60) (Fig. 2f–h). IRIS-2<sub>TMR</sub> signals did not return to its basal level during the intervals between Ca<sup>2+</sup> transients, and its fluctuation was synchronous with Ca<sup>2+</sup> oscillations (Fig. 2f). These characteristic IP<sub>3</sub> dynamics monitored with IRIS-2<sub>TMR</sub> in HeLa cells are almost same as those recorded with other FRET-based IP<sub>3</sub> sensors<sup>15,25,29,30</sup>.

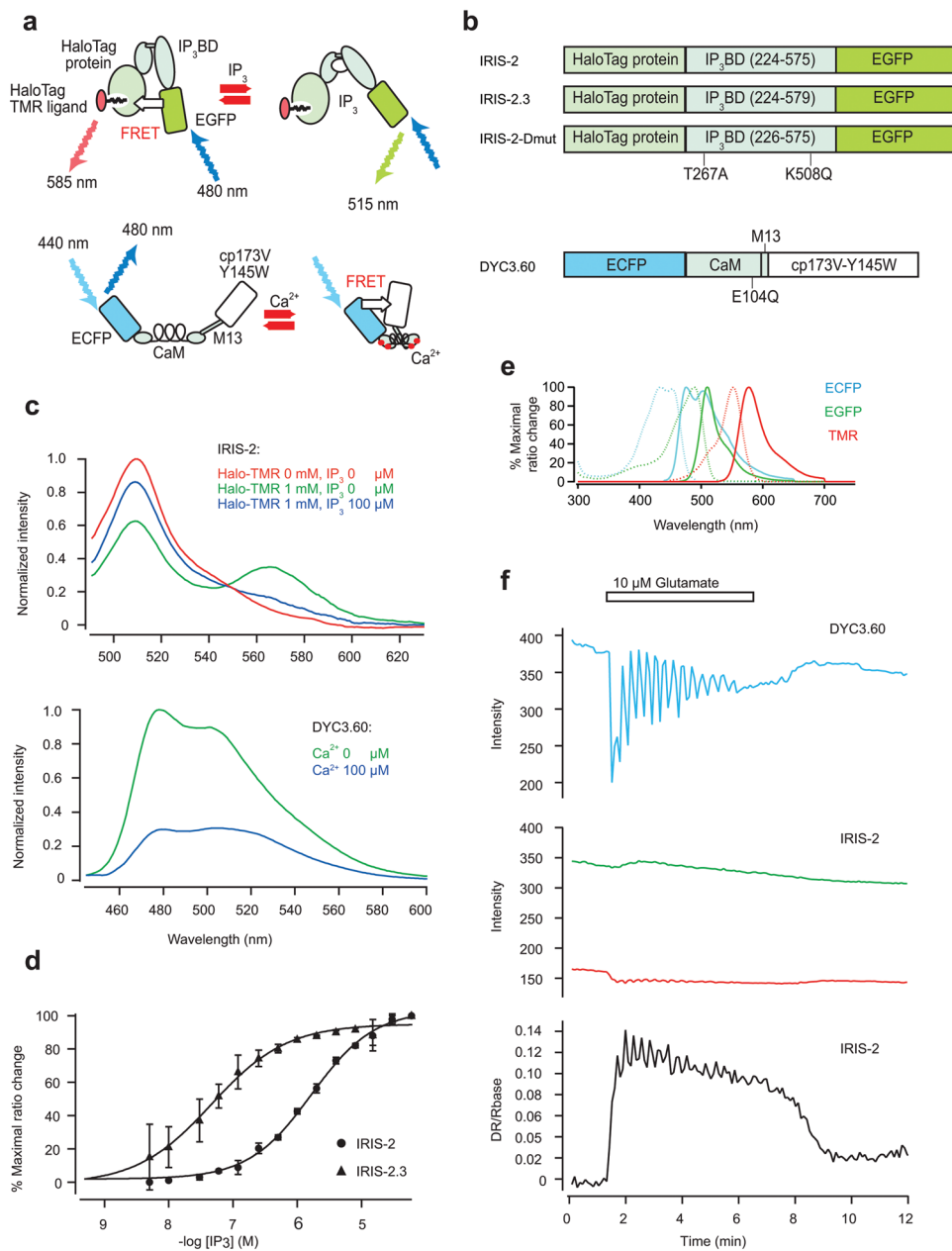


**Figure 1.** Construction and characterization of IRIS-2s and DY3.60. **(a)** Schematic drawing of IRIS-2s and DY3.60. IRIS-2s are composed of the IP<sub>3</sub>BD of mouse IP<sub>3</sub>R1, EGFP and HaloTag protein. HaloTag TMR ligand was used for the acceptor in IRIS-2s. DY3.60 is composed of calmodulin (CaM), M13 peptide, ECFP and a non-fluorescent mutant of circularly permuted Venus (cp173V-Y145W). **(b)** Domain structures of IRIS-2 proteins and DY3.60. **(c)** Emission spectra of IRIS-2 (upper panel) and DY3.60 (lower panel) excited at 480 and 440 nm, respectively. Spectra of purified IRIS-2 (red line), IRIS-2<sub>TMR</sub> (in the presence of 1 μM HaloTag TMR ligand) (green line), and IRIS-2<sub>TMR</sub> in the presence of 100 μM IP<sub>3</sub> (blue line). Spectra of lysate of DY3.60-expressing COS7 cells were measured with 0.1 mM of CaCl<sub>2</sub> (blue line) or without CaCl<sub>2</sub> (green line). **(d)** Apparent IP<sub>3</sub> affinities of purified IRIS-2<sub>TMR</sub> (circles) and IRIS-2.3<sub>TMR</sub> (triangles). Data were obtained from three independent measurements. Error bars correspond to the SD. **(e)** Excitation (broken lines) and emission (continuous lines) spectra of ECFP, EGFP, and TMR. **(f)** Time courses of emission changes of DY3.60 (blue line), EGFP (green line) and TMR (red) of IRIS-2<sub>TMR</sub> in mGluR5 expressing HeLa cells stimulated with 10 μM glutamate (horizontal bars). The ratio of EGFP and TMR is drawn in the bottom panel (black line).

**Initiation, maintenance, and termination of Ca<sup>2+</sup> oscillations in HeLa cells.** Figure 2i–k show imaging data of IRIS-2 and DY3.60 in mGluR5-expressing HeLa cells. The dual FRET imaging clearly showed [IP<sub>3</sub>] increase precedes [Ca<sup>2+</sup>] rise as same as our previous report with IRIS-1<sup>25</sup> (Fig. 2i,j). Figure 2k shows a phase plane trajectory of [IP<sub>3</sub>] and [Ca<sup>2+</sup>] imaging data. [IP<sub>3</sub>] gradually increased from 1st to 4th Ca<sup>2+</sup> spikes, and then,

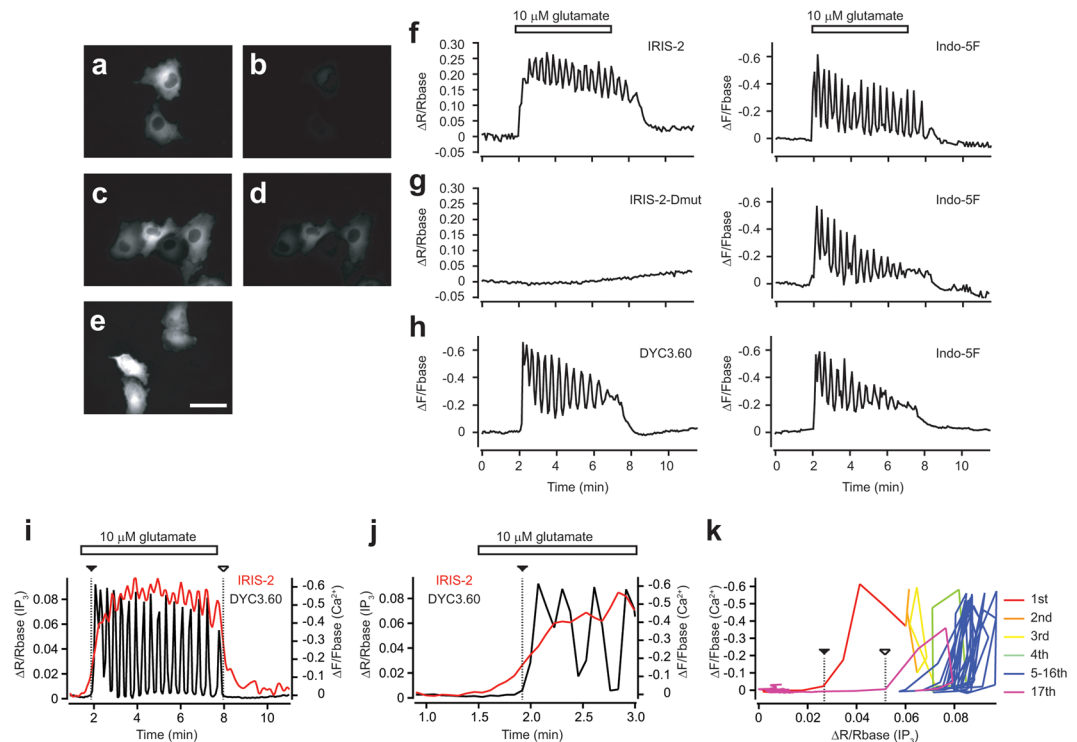


**Figure 2.** Effect of FRET sensors to  $[Ca^{2+}]$  dynamics in HeLa cells. (a–d) Fluorescent images of IRIS-2 expressing cells without (a,b) and with HaloTag TMR staining (c,d). Bar, 50  $\mu$ m. Emissions detected by filters for GFP are shown in (a,c). Emissions detected by filters for TMR are shown in (b,d). (e) A fluorescent image of DYC3.60 expressing cells. (f–h) Effect of FRET sensors to  $[Ca^{2+}]$  dynamics in HeLa cells. Cells expressing IRIS-2 (f), IRIS-2-Dmut (g), or DYC3.60 (h) were stained with HaloTag TMR and Indo-5F. Left panels are time courses of emission ratio (f,g) or emission (h) changes of FRET sensors in mGluR5 expressing HeLa cells stimulated with 10  $\mu$ M glutamate (horizontal bars). Right panels are time courses of emission changes of Indo-5F in the same cells of left panels. (i–k)  $[IP_3]$  and  $[Ca^{2+}]$  changes were imaged with the dual FRET probes. Initiation of the first  $Ca^{2+}$  spike and the termination of  $Ca^{2+}$  oscillations were marked with dashed line with closed and open triangles, respectively. (j)  $[IP_3]$  and  $[Ca^{2+}]$  changes around the rise of first  $Ca^{2+}$  spike. (k) A phase plane trajectory is drawn with  $[IP_3]$  and  $[Ca^{2+}]$  imaging data.

repeated  $Ca^{2+}$  spikes occurred in the certain range of  $[IP_3]$  (Fig. 2k). In the range of  $[IP_3]$ , the trajectory cycled at almost the same orbit, suggesting that the trajectory is in a limit cycle (Fig. 2k). After termination of agonist stimulation,  $[IP_3]$  decreased below the range of limit cycle maintenance, which resulted in the termination of  $Ca^{2+}$  oscillations (Fig. 2i,k). In the initial phase of  $Ca^{2+}$  oscillations,  $[IP_3]$  increase precedes  $Ca^{2+}$  spikes (Fig. 2k), suggesting that  $[IP_3]$  increases induce  $Ca^{2+}$  spikes. In the limit cycle phase,  $Ca^{2+}$  spikes occur without marked  $[IP_3]$  increases (Fig. 2k), suggesting that  $Ca^{2+}$  induced positive and negative feedbacks to  $IP_3R$  autonomously induce  $Ca^{2+}$  spikes<sup>24</sup>.  $Ca^{2+}$  oscillations last as long as  $[IP_3]$  maintained in the range of limit cycle. Termination of agonist stimulation induces  $[IP_3]$  decrease below to the range maintaining the limit cycle.  $[IP_3]$  necessary to induce  $Ca^{2+}$  spike should be different at the initial state and later state of  $Ca^{2+}$  oscillations because  $Ca^{2+}$  directly or indirectly inactivates  $IP_3R$ <sup>28,31</sup>. Thus,  $Ca^{2+}$  disappears even  $[IP_3]$  above the basal level at the termination of  $Ca^{2+}$  oscillations (Fig. 2i).

**Characterization of IRIS-2 in UV-uncaging experiments.** Next, we checked the compatibility of  $IP_3$  sensors with UV-uncaging. Caged-compounds are light-sensitive probes that functionally encapsulated biomolecules in an inactive form. The active compounds can be released from caged-compounds with UV light in most of caged-compounds. IRIS-1 or IRIS-2 were expressed in HeLa cells and irradiated by UV pulses (Supplementary Fig. 2a,b). We found UV irradiation caused temporal reduction of fluorescence of both ECFP and Venus in IRIS-1 expressing cells (Supplementary Fig. 2a). Because of the difference of the signal reduction between those fluorescent proteins, the fluorescent ratio of IRIS-1 was significantly reduced ( $-1.9 \pm 0.7\%$ ,  $n = 22$ ). In contrast, the fluorescent signals from EGFP and HaloTag-TMR were stable after the UV irradiation (Supplementary Fig. 2b), which resulted in successful detection of  $[IP_3]$  changes after UV-uncaging of caged- $IP_3$  (Supplementary Fig. 2c).

**Detection of  $IP_3$  concentration changes in fertilized mouse eggs.** To detect  $IP_3$  dynamics in fertilized mouse eggs, IRIS-1, IRIS-2, or IRIS-2.3 was expressed in eggs by cRNA injection. For the simultaneous monitoring of  $[Ca^{2+}]$  changes, we first used Indo-5F as a  $Ca^{2+}$  indicator according to the method described previously<sup>25</sup>. As shown in Supplementary Figure 3, we did not detect any changes of IRIS-1 signals in fertilized eggs. Not only the fails of the detection of  $IP_3$  changes, it was difficult to detect  $[Ca^{2+}]$  changes after addition of

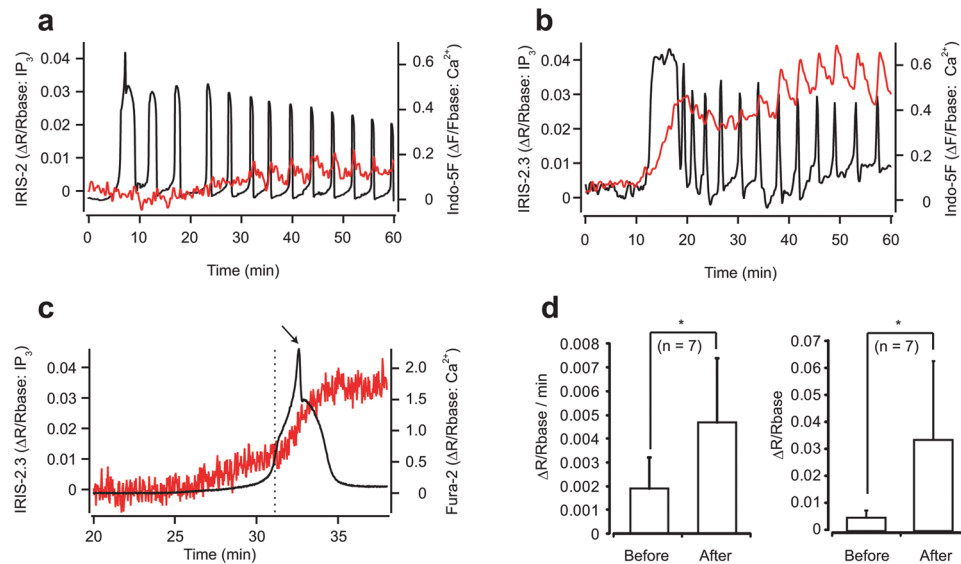


**Figure 3.** IRIS-2<sub>TMR</sub> and IRIS-2.3<sub>TMR</sub> signals in fertilized mouse eggs. **(a,b)**  $[IP_3]$  and  $[Ca^{2+}]$  dynamics detected by IRIS-2s and Indo-5F. Normalized emission ratio changes ( $\Delta R/R_{base}$ ) of IRIS-2<sub>TMR</sub> **(a)** and IRIS-2.3<sub>TMR</sub> **(b)** are plotted with red lines.  $[Ca^{2+}]$  changes detected with Indo-5F are shown with black lines **(a,b)**. Sperm was added at time zero **(a,b)**. Fluorescent images were acquired each 4 sec in **(a)** and each 10 sec in **(b)**. **(c)** Time courses of emission ratio changes of Fura-2 (black) and IRIS-2.3<sub>TMR</sub> (red) at a first  $Ca^{2+}$  spike after fertilization. The average values from whole egg were plotted against time. A peak of the first  $Ca^{2+}$  spike is shown by an arrow. The time point of the change in the rate of rise in the IRIS-2.3<sub>TMR</sub> signal is shown by a vertical broken line. **(d)** Left panel shows the rates of  $[IP_3]$  increases before and after the shoulder point of the first  $Ca^{2+}$  spike. Right panel shows peak  $[IP_3]$  change before  $[Ca^{2+}]$  rise and first  $[IP_3]$  peak after  $[Ca^{2+}]$  rise.  $n = 7$ .  $*p < 0.05$ , Student's t-test.

sperm into the culturing media. Even in the experiments with successful detection of fertilization-induced  $[Ca^{2+}]$  changes, the number of  $Ca^{2+}$  transients was less compared to IRIS-2-Dmut (number of  $Ca^{2+}$  spikes during 30 min after the first  $Ca^{2+}$  spikes: IRIS-1:  $1.91 \pm 0.13$  ( $n = 3$ ); IRIS-1-Dmut:  $3.75 \pm 0.5$  ( $n = 4$ );  $p = 0.008$ , Student's t-test), suggesting that IRIS-1 works as a significant  $IP_3$  buffer. We also tested IRIS-2 expressing eggs for *in-vitro* fertilization assay and found IRIS-2 expressing eggs had normal  $Ca^{2+}$  spikes after fertilization (Fig. 3a). However, it was also hard to detect clear increases in FRET signals in IRIS-2-expressing eggs during the first  $Ca^{2+}$  transient evoked after fertilization, while small repetitive transients of IRIS-2<sub>TMR</sub> signals synchronous with  $Ca^{2+}$  oscillations were observed approximately 30 min after the onset of the first  $Ca^{2+}$  transient (Fig. 3a). On the other hand, we clearly detected  $IP_3$  increases during the all  $Ca^{2+}$  transients, including the first  $Ca^{2+}$  transient, in IRIS-2.3-expressing eggs (Fig. 3b). During the first large  $Ca^{2+}$  transient,  $[IP_3]$  continues to increase, and all the following  $Ca^{2+}$  transients accompanied with a rapid increase and a following slow decline on the elevated level of  $[IP_3]$  (Fig. 3b). Three independent experimental results of  $[IP_3]$  and  $[Ca^{2+}]$  imaging with IRIS-2.3 and Indo-5F at the onset of first  $Ca^{2+}$  spike were shown in Supplementary Figure 4. We did not find significant difference of numbers of  $Ca^{2+}$  spikes during 30 min after 1st  $Ca^{2+}$  spike between IRIS-2 and IRIS-2.3 expressing eggs (IRIS-2:  $5.17 \pm 1.72$ ,  $n = 6$ ; IRIS-2.3:  $6.33 \pm 5.72$ ,  $n = 9$ ;  $p = 0.58$ , student's t-test).

**Initiation of  $[IP_3]$  and  $[Ca^{2+}]$  changes.** Next, we investigated the temporal order of the onset of increase between  $[IP_3]$  changes and  $[Ca^{2+}]$  changes during the first  $Ca^{2+}$  transient evoked after fertilization. To detect the initial  $[Ca^{2+}]$  changes experimentally, we used Fura-2, whose affinity is higher than that of Indo-5F (Fura-2:  $K_d = 135$  nM; Indo-5F:  $K_d = 470$  nM), as a  $Ca^{2+}$  indicator to detect the timing of the onset of the first  $Ca^{2+}$  transient as precise as possible. As shown in Fig. 3c,  $[IP_3]$  rise preceded the onset of the initial step of the first  $Ca^{2+}$  transient for  $2.7 \pm 2.4$  min in 11 of 13 eggs. The initial  $[IP_3]$  increase should initiate  $Ca^{2+}$  release from  $IP_3R$ .  $IP_3$  and  $Ca^{2+}$  are the co-agonist of  $IP_3R$ , and open probability of  $IP_3R$  markedly increase with  $Ca^{2+}$  in the presence of  $IP_3$ <sup>32</sup>. Thus,  $Ca^{2+}$ -induced  $Ca^{2+}$  release (CICR) from  $IP_3R$  should have major role to produce initial  $Ca^{2+}$  spike. The first  $Ca^{2+}$  transient observed in IRIS-2.3-expressing eggs was composed of two steps separated by a shoulder point (dashed line in Fig. 3c) as reported previously<sup>33</sup>. The peak amplitude and the rising speed of  $[IP_3]$  increased after the shoulder point of the first  $Ca^{2+}$  transient (Fig. 3c,d), suggesting acceleration of  $IP_3$  production via  $Ca^{2+}$ -induced activation of PLC isozymes.

**Positive feedback loop to produce rising phase of  $Ca^{2+}$  spikes.** Each  $Ca^{2+}$  spike of  $Ca^{2+}$  oscillations usually form as a result of an initial slow pacemaker rise in  $[Ca^{2+}]$  followed by a rapid rise in  $[Ca^{2+}]$ <sup>34–36</sup>. The accelerated rise of  $[Ca^{2+}]$  is suggested that a regenerative process is involved in the generation of the abrupt upstroke<sup>35</sup>. Such regenerative processes require a positive-feedback element<sup>22</sup>, and CICR from  $IP_3R$  and  $Ca^{2+}$ -induced  $IP_3$  production through PLC have been proposed as candidates of the positive feedback element. In the previous

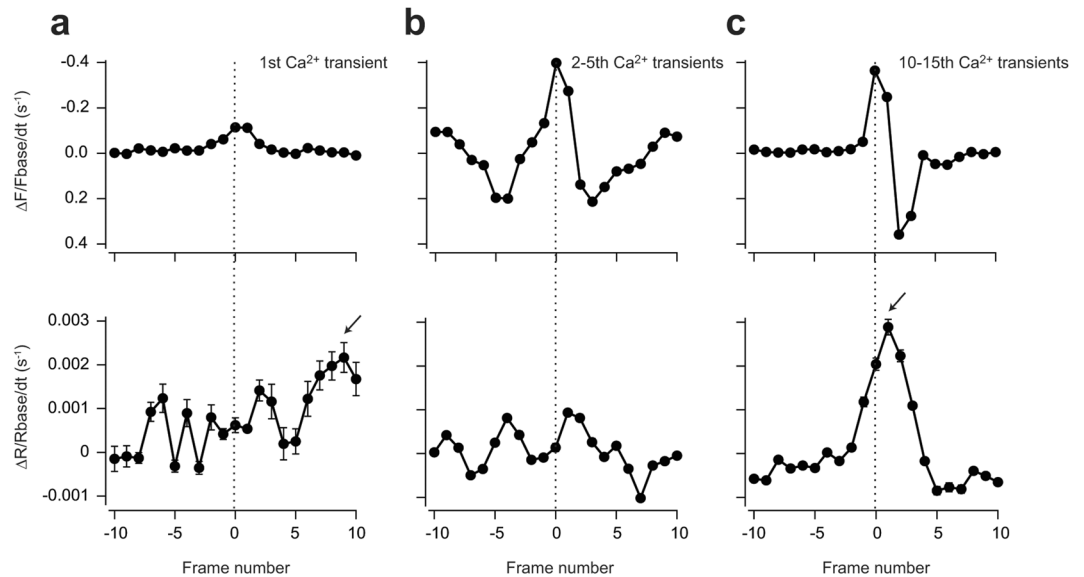


**Figure 4.** Rate of  $[Ca^{2+}]$  and  $[IP_3]$  changes at each  $Ca^{2+}$  spike. Rate of  $[Ca^{2+}]$  and  $[IP_3]$  changes are shown as differentiated signals of Indo-5F (Em. 460–510 nm) (upper panel) and IRIS-2.3<sub>TMR</sub> (lower panel) aligned by the time when the differentiated Indo-5F signal was at its maximum (frame 0, broken line) during first  $Ca^{2+}$  transients after fertilization ( $n=9$ ) (a), from 2nd to 5th  $Ca^{2+}$  transients ( $n=20$ ) (b) and from 10th to 15th  $Ca^{2+}$  transients ( $n=20$ ) (c). Error bars correspond to the SD. Arrowheads indicate the peak of the rate of  $[IP_3]$  rise. Broken vertical lines indicate the peaks of differentiated Indo-5F signals.

study, we compared rate of  $[IP_3]$  and  $[Ca^{2+}]$  rises at the onset of  $Ca^{2+}$  spikes and found each  $Ca^{2+}$  spike is not accompanied by acceleration in the rate of increase in  $IP_3$  in HeLa cells<sup>25</sup>. As same as HeLa cells, if the regenerative  $IP_3$  production mediated by PLC activated by cytosolic  $Ca^{2+}$  drives the rising phase of  $Ca^{2+}$  spikes, the rate of  $[IP_3]$  rise should accelerate when the rate of  $[Ca^{2+}]$  rise accelerate. To test this possibility, the fluorescent signals of both Indo-5F and IRIS-2.3<sub>TMR</sub> were differentiated and aligned at the time when the rate of  $[Ca^{2+}]$  rise reached its maximum (Fig. 4). In the early phase (from first to 5th transients) of fertilization-induced  $Ca^{2+}$  oscillations, the amplitudes of  $IP_3$  fluctuations were relatively small (Fig. 3b), and the rate of  $[IP_3]$  rise did not increase during the rising phase of the  $Ca^{2+}$  transients, as found in cultured HeLa cells<sup>25</sup> (Fig. 4a,b). The amplitudes of  $IP_3$  fluctuations were gradually increased during the later phase of  $Ca^{2+}$  oscillations (Fig. 3a,b), and contrary to the early phase, the onset of the rate of  $[IP_3]$  rise precedes that of  $[Ca^{2+}]$  (Fig. 4c). The result suggests that  $Ca^{2+}$ -induced  $IP_3$  production through PLC may work as a part of the positive feedback loop to produce abrupt  $[Ca^{2+}]$  rise at  $Ca^{2+}$  spikes in later phase of  $Ca^{2+}$  oscillations. However, the peak of the rate of  $[IP_3]$  rise always delayed from that of  $[Ca^{2+}]$  (Fig. 4c), suggesting that CICR from  $IP_3R$  has major role to produce the rising phase of  $Ca^{2+}$  spikes and  $[IP_3]$  rises.

$[IP_3]$  stayed at the elevated level and did not return to the basal level through  $Ca^{2+}$  oscillations (Fig. 3b).

**Dual-FRET imaging of  $[IP_3]$  and  $[Ca^{2+}]$  in fertilized mouse eggs.** We also test our dual-FRET pair for  $[IP_3]$  and  $[Ca^{2+}]$  at fertilization of mouse eggs. We microinjected cRNAs of DYIC3.60 and IRIS-2.3 into the eggs and stained the eggs with TMR. As shown in Fig. 5a, these fluorescent probes were distributed evenly in the egg. Well separation of excitation and emission spectra of these fluorophores enabled simultaneous detection of these fluorescence (Figs 1e, 5a,b). As same as the results we obtained with the pair of Indo-5F and IRIS-2.3<sub>TMR</sub>, we successfully detected fertilization-induced  $[Ca^{2+}]$  and  $[IP_3]$  changes with DYIC3.60 and IRIS-2.3<sub>TMR</sub> (Fig. 5b and Supplementary video 1). As same as HeLa cells,  $[IP_3]$  at the termination was higher than that at the initiation of  $Ca^{2+}$  oscillations in fertilized mouse eggs (Fig. 2i and Supplementary Fig. 5).

**$Ca^{2+}$ -induced regenerative  $IP_3$  production.** We also detected delays in the peak of  $[IP_3]$  compared to the peak of each  $Ca^{2+}$  spike ( $17 \pm 11$  sec,  $n=63$ , Fig. 5c,d), suggesting that  $Ca^{2+}$ -induced regenerative  $IP_3$  production through PLC produces small  $[IP_3]$  rises at each  $Ca^{2+}$  spike to maintain  $[IP_3]$  over the basal level, which results in long lasting  $Ca^{2+}$  oscillations in fertilized eggs. Which PLC isoforms contribute to this regenerative process? Eight PLC isoforms are known to express in the mouse egg: PLC $\beta$ 1<sup>37</sup>, PLC $\beta$ 3<sup>37</sup>, PLC $\beta$ 4<sup>23</sup>, PLC $\gamma$ 1<sup>37</sup>, PLC $\gamma$ 2<sup>37</sup>, PLC $\delta$ 1<sup>23</sup>, PLC $\delta$ 4<sup>23</sup>, and PLC $\epsilon$ <sup>23</sup>. From these isoforms, knockout mice of PLC $\beta$ 4, PLC $\delta$ 1, PLC $\delta$ 4, and PLC $\epsilon$  are born normally<sup>23,38–40</sup>. On the other hand, knockout mice of PLC $\beta$ 1<sup>41</sup>, PLC $\beta$ 3<sup>42</sup>, PLC $\gamma$ 1<sup>38</sup>, and PLC $\gamma$ 2<sup>43</sup> have problems on development of the embryo. However, dominant-negative experiments employing recombinant SH2 domain to inhibit PLC $\gamma$ 1 and  $\gamma$ 2 did not inhibit the  $Ca^{2+}$  oscillatory pattern during fertilization<sup>44</sup>. Based on these findings, Igarashi *et al.* found that reduced expression of PLC $\beta$ 1 by RNAi resulted in a significant decrease in  $Ca^{2+}$  transients and overexpression of PLC $\beta$ 1 by cRNA injection resulted in perturbed duration and frequency of  $Ca^{2+}$  oscillations<sup>23</sup>. Thus,  $Ca^{2+}$  induced activation of PLC $\beta$  isozymes are the strong candidates which play a pivotal role to the accelerated production of  $IP_3$  during  $Ca^{2+}$  spikes in fertilized mouse eggs. To determine the role of PLC $\beta$  in

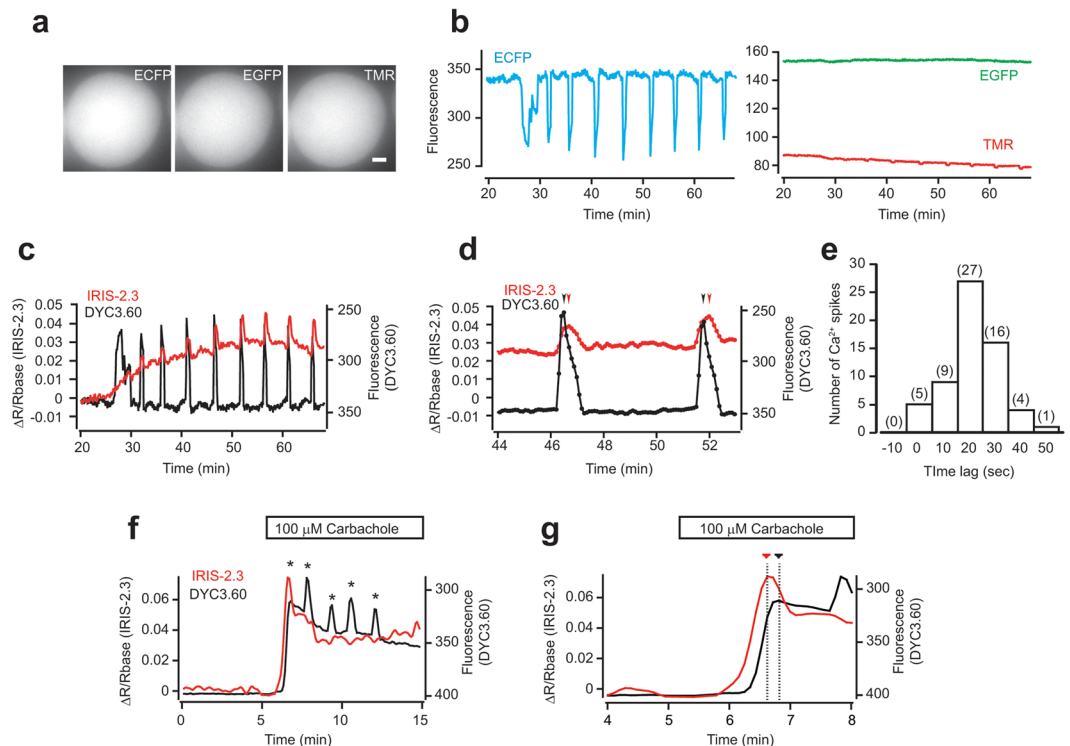


**Figure 5.** Delayed  $\text{IP}_3$  pulses during  $\text{Ca}^{2+}$  oscillations in fertilized mouse eggs visualized by dual-FRET sensors. (a) Fluorescence images of DY3.60 (ECFP) and IRIS-2.3<sub>TMR</sub> (EGFP and TMR) in a single mouse egg. DY3.60 was illuminated with 425–445 nm light, and IRIS-2.3<sub>TMR</sub> was illuminated with 460–490 nm light. Scale bar, 10  $\mu\text{m}$ . (b) Dual-FRET imaging of  $[\text{IP}_3]$  and  $[\text{Ca}^{2+}]$  in a fertilized mouse egg. Signals from DY3.60 (ECFP) and IRIS-2.3<sub>TMR</sub> (EGFP and TMR) from single fertilized mouse egg are shown in the left and right panels, respectively. (c) Emission changes in DY3.60 (black line) and ratio changes of IRIS-2.3<sub>TMR</sub> (red line) are shown. Sperm was added at time zero. (d) Data shown in (c) on an enlarged time scale. The arrowheads indicate the time of peaks in DY3.60 signal (black) and IRIS-2.3<sub>TMR</sub> signal (red). (e) A histogram of the peak time difference between DY3.60 signals and IRIS-2.3<sub>TMR</sub> signals ( $n = 61$ ). The positive value indicates that the peak of DY3.60 signals precedes that of IRIS-2.3<sub>TMR</sub> signals ( $17 \pm 11$  sec). (f) Emission ratio changes of DY3.60 (black line) and IRIS-2.3<sub>TMR</sub> (red line) in an unfertilized egg stimulated with 100  $\mu\text{M}$  carbachole. Asterisks show the peak of each  $\text{Ca}^{2+}$  spike. Carbachole was added during the time indicated by the horizontal bar. (g) Data shown in (f) on an enlarged time scale around the rise of first  $\text{Ca}^{2+}$  spike. The dashed lines with red and black triangles indicate the time of peaks in IRIS-2.3<sub>TMR</sub> signal and DY3.60 signal, respectively.

the mouse egg, we stimulate unfertilized mouse eggs with 100  $\mu\text{M}$  carbachole (Fig. 5f,g). The stimulation caused  $\text{Ca}^{2+}$  spikes and a monotonic  $[\text{IP}_3]$  rise (Fig. 5f). At fertilization,  $[\text{IP}_3]$  changes always follow after  $\text{Ca}^{2+}$  spikes. On the other hand,  $\text{Ca}^{2+}$  spikes did not accompany with delayed  $[\text{IP}_3]$  rises in carbachole stimulated unfertilized eggs (Fig. 5f). Particularly,  $\text{IP}_3$  peak at the first  $\text{Ca}^{2+}$  spike preceded  $\text{Ca}^{2+}$  peak (Fig. 5g). These data showed that  $\text{Ca}^{2+}$ -induced  $\text{IP}_3$  producing activity is not strong in unfertilized eggs, suggesting that sperm derived PLC $\zeta$  should participate  $\text{Ca}^{2+}$ -induced  $\text{IP}_3$  production. As we showed in Figs 3a,b and 4,  $\text{Ca}^{2+}$ -induced  $[\text{IP}_3]$  rises increased later phase of fertilization-induced  $\text{Ca}^{2+}$  oscillations, suggesting that fertilization induces quantitative or qualitative changes of PLC in later phase of  $\text{Ca}^{2+}$  oscillations.

## Discussion

In this study, we developed a dual-FRET pair of biosensors for the detection of  $[\text{IP}_3]$  and  $[\text{Ca}^{2+}]$  in mammalian cells. The uniqueness of our dual-FRET pair is using single fluorophore for one of the pairs. Replacement of Y145 to W in EYFP is known to produce a non-fluorescent chromoprotein that retains its absorption of emission light<sup>26</sup>. Introduction of the Y145W mutation into cp173Venus of YC3.60<sup>27</sup> resulted to produce single fluorophore with fluorescent quencher in the  $\text{Ca}^{2+}$  FRET sensor, DY3.60. Usually, four fluorophores are necessary for dual-FRET imaging. Most of FRET sensors have cyan and yellow fluorescent proteins<sup>45</sup>, and these fluorescent proteins cover a broad spectral profile. Thus, using FRET sensor with cyan and yellow proteins, it is difficult to find a partner FRET sensor for dual-FRET imaging without using spectral unmixing to distinguish each fluorescent signal mathematically from significantly overlapped fluorescent signals<sup>46,47</sup>. We offer a dual-FRET imaging with three fluorophores, which gives easier detection and separation of fluorescent signals.

The new FRET sensors enabled imaging of  $[\text{IP}_3]$  and  $[\text{Ca}^{2+}]$  at fertilization of mouse eggs. We have succeeded to detect  $[\text{IP}_3]$  changes in fertilized mouse eggs using a second-generation fluorescent  $\text{IP}_3$  sensor, IRIS-2.3, which has an improved dynamic range and a high  $\text{IP}_3$  sensitivity. Simultaneous monitoring of both  $\text{Ca}^{2+}$  and  $\text{IP}_3$  in fertilized mouse eggs showed that the  $[\text{IP}_3]$  increase was detected approximately 3 min before the onset of the first

Ca<sup>2+</sup> transient. The result is consistent with the expectation that highly Ca<sup>2+</sup> sensitive PLC $\zeta$  produces IP<sub>3</sub> at the basal level of [Ca<sup>2+</sup>] in the egg cytosol after sperm-egg fusion<sup>12</sup>. Mehlmann and Kline reported microinjection of small amount of IP<sub>3</sub> (8.6 nM) is able to induce Ca<sup>2+</sup> spike in unfertilized mouse eggs<sup>48</sup>. Our measurements showed the same results that the amount of IP<sub>3</sub> produced in mouse eggs is small even after the fertilization because only IRIS-2.3, which shows the highest IP<sub>3</sub> sensitivity (Kd = 47 nM) among the IP<sub>3</sub> sensors developed, could detect [IP<sub>3</sub>] increases at the onset of the first Ca<sup>2+</sup> transients.

IP<sub>3</sub>R has a bell-shaped calcium response curve: the open probability of IP<sub>3</sub>R is activated by low [Ca<sup>2+</sup>] and inhibited by high [Ca<sup>2+</sup>]<sup>32</sup>. Based on this finding, De Young and Keizer reported a mathematical model to reproduce Ca<sup>2+</sup> oscillations with constant [IP<sub>3</sub>]<sup>24</sup>. In this and previous reports, we showed sustained [IP<sub>3</sub>] increase during Ca<sup>2+</sup> oscillations in HeLa cells and fertilized mouse eggs<sup>25</sup> (Figs 3 and 4), and the same results were obtained with other IP<sub>3</sub> sensor proteins<sup>29,30</sup>. Consistently with our results, Mehlmann and Kline reported single microinjection of IP<sub>3</sub> induces Ca<sup>2+</sup> oscillations in unfertilized mouse eggs<sup>48</sup>. Jones *et al.* also reported Ca<sup>2+</sup> oscillations with continuous low level caged-IP<sub>3</sub> photolysis in unfertilized mouse eggs<sup>49</sup>. PLC $\zeta$  is a smallest and simplest PLC isoform<sup>9</sup>. The activity of PLC $\zeta$  is regulated by Ca<sup>2+</sup> and localization into nucleus after pronuclear formation, and other regulations are not known<sup>50</sup>. PLC $\zeta$  has highest Ca<sup>2+</sup> sensitivity compared to the other PLC isoforms and is 70% active at the basal level [Ca<sup>2+</sup>] in cells<sup>12</sup>. Thus, PLC $\zeta$  should be continuously active after fertilization until pronuclear formation<sup>51</sup>, which should sustain continuous [IP<sub>3</sub>] increase during fertilization-induced Ca<sup>2+</sup> oscillations (Figs 3 and 4). We previously found that CICR dominantly work as a positive feedback loop to produce the rising phase of Ca<sup>2+</sup> spikes in HeLa cells<sup>25</sup>. Our data suggest that the mechanism elicits the rising phase of Ca<sup>2+</sup> spikes in fertilized mouse eggs is more complex. Initially, CICR dominantly works as the positive feedback loop, and Ca<sup>2+</sup>-induced IP<sub>3</sub> production gradually participates to produce Ca<sup>2+</sup> spikes cooperatively with CICR in the later phase of Ca<sup>2+</sup> oscillations. Ca<sup>2+</sup>-induced IP<sub>3</sub> production through PLC produces [IP<sub>3</sub>] rises at each Ca<sup>2+</sup> spike to help keeping [IP<sub>3</sub>] over the basal level, which results in long lasting Ca<sup>2+</sup> oscillations in fertilized eggs.

In conclusion, we produced FRET sensors with new choices of fluorophores for dual-FRET imaging of [IP<sub>3</sub>] and [Ca<sup>2+</sup>]. Less overlaps of excitation and emission spectrum of IRIS-2s and DY3.60 allowed dual-FRET imaging of Ca<sup>2+</sup> and IP<sub>3</sub> even without spectral unmixing. Because of the smaller number of fluorophores, our dual-FRET approach can reduce the effort to detect each fluorescent signal separately. The wider dynamic range and higher sensitivity achieved by IRIS-2.3 will enable the detection of subtle [IP<sub>3</sub>] changes associated with [Ca<sup>2+</sup>] changes at egg fertilization to local [Ca<sup>2+</sup>] increase events.

## Materials and Methods

**Animals.** Experiments used ddY mice for preparation of oocytes and sperm. All animal experiments were performed in accordance with the guidelines approved by the Animal Experiments Committee of RIKEN Brain Science Institute. All experiments were carried out in accordance with the approved ethical guidelines and regulations.

**Gene construction.** The FRET donor and acceptor of IRIS-1 were replaced with mEGFP and Halo-protein (Promega), respectively, to produce IRIS-2. Amino acid residues 224–575 of mouse IP3R1 in IRIS-2 were replaced with amino acid residues 224–579 of mouse IP3R1 to produce IRIS-2.3. The Y145W mutant<sup>26</sup> of circular permuted Venus (cp173V-Y145W)<sup>27</sup> was generated using the site-directed mutagenesis. The FRET acceptor of YC3.60<sup>27</sup> was replaced with cp173Venus-Y145W to produce DY3.60. IRIS-2, IRIS-2.3 and DY3.60 cDNAs were cloned into the NheI and XbaI sites of pcDNA3.1 zeo(+) (Invitrogen) for the expression in HeLa cells. The cDNAs were cloned into the XbaI site of pTNTM (Promega) with extended poly(A) tail (57 residues) and synthesized cRNAs were injected into mouse oocytes.

**Protein expression and purification.** The full-length cDNA of IRIS-2 was isolated from pcDNA3.1 zeo(+)-IRIS-2 by using NheI and XbaI sites and was cloned into the XbaI site of baculovirus transfer vector pFast-Bac1 (Invitrogen). The recombinant baculovirus was used for the large-scale expression of IRIS-2 in Sf9 cells as described previously<sup>52</sup>. The expressed proteins were purified on a HiTrap heparin HP column (GE Healthcare Life Sciences) as described previously<sup>53</sup>.

**Cell culture and transfection.** HeLa cells were cultured in Dulbecco's modified Eagle medium supplemented with 10% heat-inactivated fetal bovine serum. HeLa cells were transfected with expression vectors by transfection reagent (Mirus TransIT). One day after the transfection, cells were used for imaging experiments.

**Preparation of RNA.** Plasmids carrying IRISs or DY3.60 were digested by NdeI, and linearized DNA fragments were purified with Wizard SV Gel and PCR clean-up Kit (Promega). They were used as the templates for RNA transcription by T7 polymerase using T7 mMESSEGE MACHINE Kit (Ambion). RNA was purified using RNeasy MinElute Cleanup Kit (Qiagen) and stored at –80 °C until use.

**Preparation of gametes.** Full grown immature oocytes were collected from the follicles in the ovaries of female mice 47–49 h after the injection of pregnant mare serum gonadotropin. Isolated oocytes were freed from cumulus cells mechanically by pipetting in M2 medium, and then cRNAs of IRIS-1, IRIS-2, IRIS-2.3, DY3.60 or dKeima570 were injected as described below. Sperm was collected from the caudal epididymides and were incubated in M16 medium<sup>54</sup> supplemented with 4 mg/ml BSA (Sigma) at 37 °C (5% CO<sub>2</sub>) for >5 h for capacitation and acrosome reaction<sup>55</sup>.

**Microinjection and insemination.** RNA solutions were diluted to 130 ng/μl with the intracellular medium (150 mM KCl, 5 mM Tris-KOH, pH 7.0). Immature oocytes were injected with 20 pl of RNA solutions and incubated in the M16 medium for 16 h at 37 °C with 5% CO<sub>2</sub>. Only eggs matured normally to metaphase II with the



first polar body were used in the following experiments. After loaded with 2  $\mu\text{M}$  of Indo-5F or Fura-2 for 30 min in the M2 medium, eggs were freed from the zona pellucida by brief treatment with acidic Tyrode's solution (pH 2.5)<sup>56</sup> for insemination. Sperm was added during imaging experiments.

**Imaging.** After loading HeLa cells with 10  $\mu\text{M}$  Indo-5F-AM (AnaSpec), imaging was performed under the constant flow (2 ml/min) of the balanced salt solution containing 20 mM Hepes, pH 7.4, 115 mM NaCl, 5.4 mM KCl, 1 mM MgCl<sub>2</sub>, 1.3 mM CaCl<sub>2</sub>, and 10 mM glucose as an imaging media at 37 °C through an inverted microscope (IX71 or IX81; Olympus) with a cooled charge-coupled device (CCD) camera (ORCA-ER; Hamamatsu Photonics) and a 40x, 1.35 NA, oil-immersion objective (Olympus). For the fluorescent images of IRIS-1 and Indo-5F, an emission splitter (W-view; Hamamatsu Photonics) was used with a light source exchanger (DG-4; Sutter Instrument Co.) on the IX71 inverted microscope. Sequential excitation of IRIS-1 and Indo-5F was performed by using a 450-nm dichroic mirror and two excitation filters (a 425–445 nm filter for IRIS-1 and a 360-nm filter for Indo-5F). Emissions from IRIS-1 and Indo-5F were split with a 460–510-nm filter (for IRIS-1 and Indo-5F), a long-path 520-nm (for IRIS-1) barrier filter, and two 505-nm dichroic mirrors equipped in W-view.

Eggs were incubated with M2 buffer at 37 °C on IX81 inverted microscope. Ca<sup>2+</sup> and IP<sub>3</sub> were visualized with sets of Indo-5F and IRIS-1, Indo-5F and IRIS-2, Indo-5F and IRIS-2.3, Fura-2 and IRIS-2.3, or DY3.60 and IRIS-2.3, respectively. Sequential excitation of Ca<sup>2+</sup> and IP<sub>3</sub> indicators was performed by using dichroic mirrors (a 400-nm mirror for Indo-5F and a 450-nm mirror for IRIS-1 and DY3.60 and a 505-nm mirror for IRIS-2 and IRIS-2.3) and excitation filters (a set of 340 and 380-nm filters for Fura-2 and a 380-nm filter for Indo-5F and a 425–445 nm filter for IRIS-1 and DY3.60 and a 460–490-nm filter for IRIS-2 and IRIS-2.3). Emissions from Ca<sup>2+</sup> and IP<sub>3</sub> indicators were split with emission filters (a set of 400–420 and 460–510-nm filters for Indo-5F and a set of 460–510 and 525–565 filters for IRIS-1 and DY3.60 and a 510–550 filter for Fura-2 and a set of 510–550 and 573–613-nm filters for IRIS-2 and IRIS-2.3<sub>TMR</sub>), and three filter exchangers (Lamda 10; Sutter Instruments, IX2-RFACA; Olympus).

Image acquisition was performed with MetaFluor (Molecular Devices). Data analysis was performed with MetaFluor and Igor Pro (WaveMetrics) softwares. The EGFP/TMR emission ratio (IRIS-2s), the ECFP/Venus emission ratio (IRIS-1s), the dKeima570/ECFP emission ratio (DY3.60), the 420–440 nm/460–510 nm emission ratio (Indo-1) and the ratio of 510–550 nm emission excited at 340 nm and 510–550 nm emission excited at 380 nm (Fura-2) were defined as R.  $\Delta R$  was defined as R - R<sub>base</sub>, where R<sub>base</sub> is the basal level of R. Baseline drift in each experiment was corrected with subtracting the trend line which is calculated with the line around the beginning of each experiment.

**Uncaging of caged-IP<sub>3</sub>.** HeLa cells transfected with IRIS-2 and DY3.60 were loaded with 10  $\mu\text{M}$  membrane permeable caged-IP<sub>3</sub> (iso-Ins(1,4,5)P<sub>3</sub>/PM (caged), Enzo Life Science). The uncaging stimulation was done with extra light source (mercury lamp) equipped in IX81, filtered by a 333–348-nm filter and a 400-nm dichroic mirror, illuminated the cells through 20x, 0.50 NA, water-immersion objective (Olympus).

## References

- Schultz, R. M. & Kopf, G. S. Molecular basis of mammalian egg activation. *Curr. Top. Dev. Biol.* **30**, 21–62 (1995).
- Stricker, S. A. Comparative biology of calcium signaling during fertilization and egg activation in animals. *Dev. Biol.* **211**, 157–176, <https://doi.org/10.1006/dbio.1999.9340> (1999).
- Jones, K. T. Ca<sup>2+</sup> oscillations in the activation of the egg and development of the embryo in mammals. *Int. J. Dev. Biol.* **42**, 1–10 (1998).
- Miyazaki, S., Shirakawa, H., Nakada, K. & Honda, Y. Essential role of the inositol 1,4,5-trisphosphate receptor/Ca<sup>2+</sup> release channel in Ca<sup>2+</sup> waves and Ca<sup>2+</sup> oscillations at fertilization of mammalian eggs. *Dev. Biol.* **158**, 62–78, <https://doi.org/10.1006/dbio.1993.1168> (1993).
- Swann, K. & Yu, Y. The dynamics of calcium oscillations that activate mammalian eggs. *Int. J. Dev. Biol.* **52**, 585–594, <https://doi.org/10.1387/ijdb.072530ks> (2008).
- Ducibella, T., Schultz, R. M. & Ozil, J. P. Role of calcium signals in early development. *Semin. Cell Dev. Biol.* **17**, 324–332, <https://doi.org/10.1016/j.semcdb.2006.02.010> (2006).
- Lawrence, Y., Whitaker, M. & Swann, K. Sperm-egg fusion is the prelude to the initial Ca<sup>2+</sup> increase at fertilization in the mouse. *Development* **124**, 233–241 (1997).
- Miyazaki, S. *et al.* Block of Ca<sup>2+</sup> wave and Ca<sup>2+</sup> oscillation by antibody to the inositol 1,4,5-trisphosphate receptor in fertilized hamster eggs. *Science* **257**, 251–255 (1992).
- Saunders, C. M. *et al.* PLC zeta: a sperm-specific trigger of Ca<sup>2+</sup> oscillations in eggs and embryo development. *Development* **129**, 3533–3544 (2002).
- Swann, K. A cytosolic sperm factor stimulates repetitive calcium increases and mimics fertilization in hamster eggs. *Development* **110**, 1295–1302 (1990).
- Cox, L. J. *et al.* Sperm phospholipase C $\zeta$  from humans and cynomolgus monkeys triggers Ca<sup>2+</sup> oscillations, activation and development of mouse oocytes. *Reproduction* **124**, 611–623 (2002).
- Kouchi, Z. *et al.* Recombinant phospholipase C $\zeta$  has high Ca<sup>2+</sup> sensitivity and induces Ca<sup>2+</sup> oscillations in mouse eggs. *J. Biol. Chem.* **279**, 10408–10412, <https://doi.org/10.1074/jbc.M313801200> (2004).
- Knott, J. G. *et al.* Interference reveals role for mouse sperm phospholipase C $\zeta$  in triggering Ca<sup>2+</sup> oscillations during fertilization. *Biol. Reprod.* **72**, 992–996, <https://doi.org/10.1095/biolreprod.104.036244> (2005).
- Hirose, K., Kadowaki, S., Tanabe, M., Takeshima, H. & Iino, M. Spatiotemporal dynamics of inositol 1,4,5-trisphosphate that underlies complex Ca<sup>2+</sup> mobilization patterns. *Science* **284**, 1527–1530 (1999).
- Sato, M., Ueda, Y., Shibuya, M. & Umezawa, Y. Locating inositol 1,4,5-trisphosphate in the nucleus and neuronal dendrites with genetically encoded fluorescent indicators. *Anal. Chem.* **77**, 4751–4758, <https://doi.org/10.1021/ac040195j> (2005).
- Halet, G., Tunwell, R., Balla, T., Swann, K. & Carroll, J. The dynamics of plasma membrane PtdIns(4,5)P<sub>2</sub> at fertilization of mouse eggs. *J. Cell Sci.* **115**, 2139–2149 (2002).
- Shirakawa, H., Ito, M., Sato, M., Umezawa, Y. & Miyazaki, S. Measurement of intracellular IP<sub>3</sub> during Ca<sup>2+</sup> oscillations in mouse eggs with GFP-based FRET probe. *Biochem. Biophys. Res. Commun.* **345**, 781–788, <https://doi.org/10.1016/j.bbrc.2006.04.133> (2006).
- Kelley, G. G., Reks, S. E., Ondrako, J. M., Smrcka, A. V. & Phospholipase, C. epsilon): a novel Ras effector. *EMBO J.* **20**, 743–754, <https://doi.org/10.1093/emboj/20.4.743> (2001).

19. Rebecchi, M. J. & Pentylala, S. N. Structure, function, and control of phosphoinositide-specific phospholipase C. *Physiol. Rev.* **80**, 1291–1335, <https://doi.org/10.1152/physrev.2000.80.4.1291> (2000).
20. Rhee, S. G. & Bae, Y. S. Regulation of phosphoinositide-specific phospholipase C isozymes. *J. Biol. Chem.* **272**, 15045–15048 (1997).
21. Harootyanian, A. T. *et al.* Cytosolic  $\text{Ca}^{2+}$  oscillations in REF52 fibroblasts:  $\text{Ca}^{2+}$ -stimulated  $\text{IP}_3$  production or voltage-dependent  $\text{Ca}^{2+}$  channels as key positive feedback elements. *Cell Calcium* **12**, 153–164 (1991).
22. Meyer, T. & Stryer, L. Molecular model for receptor-stimulated calcium spiking. *Proc. Natl. Acad. Sci. USA* **85**, 5051–5055 (1988).
23. Igarashi, H., Knott, J. G., Schultz, R. M. & Williams, C. J. Alterations of PLC $\beta$ 1 in mouse eggs change calcium oscillatory behavior following fertilization. *Dev. Biol.* **312**, 321–330, <https://doi.org/10.1016/j.ydbio.2007.09.028> (2007).
24. De Young, G. W. & Keizer, J. A single-pool inositol 1,4,5-trisphosphate-receptor-based model for agonist-stimulated oscillations in  $\text{Ca}^{2+}$  concentration. *Proc. Natl. Acad. Sci. USA* **89**, 9895–9899 (1992).
25. Matsu-ura, T. *et al.* Cytosolic inositol 1,4,5-trisphosphate dynamics during intracellular calcium oscillations in living cells. *J. Cell Biol.* **173**, 755–765, <https://doi.org/10.1083/jcb.200512141> (2006).
26. Ganesan, S., Ameer-Beg, S. M., Ng, T. T., Vojnovic, B. & Wouters, F. S. A dark yellow fluorescent protein (YFP)-based Resonance Energy-Accepting Chromoprotein (REACH) for Forster resonance energy transfer with GFP. *Proc. Natl. Acad. Sci. USA* **103**, 4089–4094, <https://doi.org/10.1073/pnas.0509922103> (2006).
27. Nagai, T., Yamada, S., Tominaga, T., Ichikawa, M. & Miyawaki, A. Expanded dynamic range of fluorescent indicators for  $\text{Ca}^{2+}$  by circularly permuted yellow fluorescent proteins. *Proc. Natl. Acad. Sci. USA* **101**, 10554–10559, <https://doi.org/10.1073/pnas.0400417101> (2004).
28. Shinohara, T. *et al.* Mechanistic basis of bell-shaped dependence of inositol 1,4,5-trisphosphate receptor gating on cytosolic calcium. *Proc. Natl. Acad. Sci. USA* **108**, 15486–15491, <https://doi.org/10.1073/pnas.1101677108> (2011).
29. Nezu, A., Tanimura, A., Morita, T., Shitara, A. & Tojyo, Y. A novel fluorescent method employing the FRET-based biosensor “LIBRA” for the identification of ligands of the inositol 1,4,5-trisphosphate receptors. *Biochim. Biophys. Acta* **1760**, 1274–1280, <https://doi.org/10.1016/j.bbagen.2006.04.004> (2006).
30. Remus, T. P. *et al.* Biosensors to measure inositol 1,4,5-trisphosphate concentration in living cells with spatiotemporal resolution. *J. Biol. Chem.* **281**, 608–616, <https://doi.org/10.1074/jbc.M509645200> (2006).
31. Taylor, C. W. & Tovey, S. C.  $\text{IP}(3)$  receptors: toward understanding their activation. *Cold Spring Harb. Perspect. Biol.* **2**, a004010, <https://doi.org/10.1101/cshperspect.a004010> (2010).
32. Bezprozvanny, L., Watras, J. & Ehrlich, B. E. Bell-shaped calcium-response curves of  $\text{Ins}(1,4,5)\text{P}_3$ - and calcium-gated channels from endoplasmic reticulum of cerebellum. *Nature* **351**, 751–754, <https://doi.org/10.1038/351751a0> (1991).
33. Deguchi, R., Shirakawa, H., Oda, S., Mohri, T. & Miyazaki, S. Spatiotemporal analysis of  $\text{Ca}^{2+}$  waves in relation to the sperm entry site and animal-vegetal axis during  $\text{Ca}^{2+}$  oscillations in fertilized mouse eggs. *Dev. Biol.* **218**, 299–313, <https://doi.org/10.1006/dbio.1999.9573> (2000).
34. Jacob, R., Merritt, J. E., Hallam, T. J. & Rink, T. J. Repetitive spikes in cytoplasmic calcium evoked by histamine in human endothelial cells. *Nature* **335**, 40–45, <https://doi.org/10.1038/335040a0> (1988).
35. Thomas, A. P., Renard, D. C. & Rooney, T. A. Spatial and temporal organization of calcium signalling in hepatocytes. *Cell Calcium* **12**, 111–126 (1991).
36. Bootman, M. D. & Berridge, M. J. Subcellular  $\text{Ca}^{2+}$  signals underlying waves and graded responses in HeLa cells. *Curr. Biol.* **6**, 855–865 (1996).
37. Dupont, G., McGuinness, O. M., Johnson, M. H., Berridge, M. J. & Borgese, F. Phospholipase C in mouse oocytes: characterization of beta and gamma isoforms and their possible involvement in sperm-induced  $\text{Ca}^{2+}$  spiking. *Biochem. J.* **316**(Pt 2), 583–591 (1996).
38. Nakamura, Y. *et al.* Phospholipase Cdelta1 is required for skin stem cell lineage commitment. *EMBO J.* **22**, 2981–2991, <https://doi.org/10.1093/emboj/cdg302> (2003).
39. Fukami, K. *et al.* Requirement of phospholipase Cdelta4 for the zona pellucida-induced acrosome reaction. *Science* **292**, 920–923, <https://doi.org/10.1126/science.1059042> (2001).
40. Bai, Y. *et al.* Crucial role of phospholipase Cepsilon in chemical carcinogen-induced skin tumor development. *Cancer Res.* **64**, 8808–8810, <https://doi.org/10.1158/0008-5472.CAN-04-3143> (2004).
41. Kim, D. *et al.* Phospholipase C isozymes selectively couple to specific neurotransmitter receptors. *Nature* **389**, 290–293, <https://doi.org/10.1038/38508> (1997).
42. Wang, S. *et al.* Targeted disruption of the mouse phospholipase C beta3 gene results in early embryonic lethality. *FEBS Lett.* **441**, 261–265 (1998).
43. Hashimoto, A. *et al.* Cutting edge: essential role of phospholipase C-gamma 2 in B cell development and function. *J. Immunol.* **165**, 1738–1742 (2000).
44. Mehlmann, L. M., Carpenter, G., Rhee, S. G. & Jaffe, L. A. SH2 domain-mediated activation of phospholipase Cgamma is not required to initiate  $\text{Ca}^{2+}$  release at fertilization of mouse eggs. *Dev. Biol.* **203**, 221–232, <https://doi.org/10.1006/dbio.1998.9051> (1998).
45. Hochreiter, B., Garcia, A. P. & Schmid, J. A. Fluorescent proteins as genetically encoded FRET biosensors in life sciences. *Sensors (Basel)* **15**, 26281–26314, <https://doi.org/10.3390/s151026281> (2015).
46. Niino, Y., Hotta, K. & Oka, K. Simultaneous live cell imaging using dual FRET sensors with a single excitation light. *PLoS One* **4**, e6036, <https://doi.org/10.1371/journal.pone.0006036> (2009).
47. Zhao, M., Wan, X., Li, Y., Zhou, W. & Peng, L. Multiplexed 3D FRET imaging in deep tissue of live embryos. *Sci. Rep.* **5**, 13991, <https://doi.org/10.1038/srep13991> (2015).
48. Mehlmann, L. M. & Kline, D. Regulation of intracellular calcium in the mouse egg: calcium release in response to sperm or inositol trisphosphate is enhanced after meiotic maturation. *Biol. Reprod.* **51**, 1088–1098 (1994).
49. Jones, K. T. & Nixon, V. L. Sperm-induced  $\text{Ca}^{2+}$  oscillations in mouse oocytes and eggs can be mimicked by photolysis of caged inositol 1,4,5-trisphosphate: evidence to support a continuous low level production of inositol 1,4,5-trisphosphate during mammalian fertilization. *Dev. Biol.* **225**, 1–12, <https://doi.org/10.1006/dbio.2000.9826> (2000).
50. Kashir, J., Nomikos, M. & Lai, F. A. Phospholipase C zeta and calcium oscillations at fertilisation: The evidence, applications, and further questions. *Adv. Biol. Regul.* **67**, 148–162, <https://doi.org/10.1016/j.jbior.2017.10.012> (2018).
51. Larman, M. G., Saunders, C. M., Carroll, J., Lai, F. A. & Swann, K. Cell cycle-dependent  $\text{Ca}^{2+}$  oscillations in mouse embryos are regulated by nuclear targeting of PLCzeta. *J. Cell Sci.* **117**, 2513–2521, <https://doi.org/10.1242/jcs.01109> (2004).
52. Iwai, M. *et al.* Molecular cloning of mouse type 2 and type 3 inositol 1,4,5-trisphosphate receptors and identification of a novel type 2 receptor splice variant. *J. Biol. Chem.* **280**, 10305–10317, <https://doi.org/10.1074/jbc.M413824200> (2005).
53. Natsume, T., Hirota, J., Yoshikawa, F., Furuichi, T. & Mikoshiba, K. Real time analysis of interaction between inositol 1,4,5-trisphosphate receptor type I and its ligand. *Biochem. Biophys. Res. Commun.* **260**, 527–533, <https://doi.org/10.1006/bbrc.1999.0905> (1999).
54. Whittingham, D. G. Culture of mouse ova. *J. Reprod. Fertil. Suppl.* **14**, 7–21 (1971).
55. Kumakiri, J., Oda, S., Kinoshita, K. & Miyazaki, S. Involvement of Rho family G protein in the cell signaling for sperm incorporation during fertilization of mouse eggs: inhibition by Clostridium difficile toxin B. *Dev. Biol.* **260**, 522–535 (2003).
56. Behringer, R., Gertsenstein, M., Nagy, K. & Nagy, A. *Manipulating the mouse embryo*. (Cold Spring Harbor Laboratory Press, 1986).

## Acknowledgements

We are grateful to Drs. Atsushi Miyawaki at Riken and Takeharu Nagai at Osaka University for donating YC3.60. We thank Mr. Akio Suzuki at Riken for technical help on plasmid constructions. We thank Dr. Sachiko Ishida at Riken for technical help on expression in SF-9 cells and purification of IP<sub>3</sub> sensors. We thank Dr. Tooru Takahashi at University of Electro-Communications for technical supports on microinjection experiments into mouse oocytes and *in vitro* fertilizations. This work was supported by grants from the Ministry of Education, Science, Sports and Culture of Japan to T. Matsu-ura (22770227), T. Michikawa (20370054), and K.M. (2022007).

## Author Contributions

T. Matsu-ura, K. Suzuki, K. Sugiura and A.K. invented IRIS-2 variants. T. Matsu-ura and A.M. invented DY3.60. T. Matsu-ura and H.S. established the method of the expression of IP<sub>3</sub> sensors in mouse eggs. T. Matsu-ura performed other experiments. T. Matsu-ura and H.S. analyzed data. T. Matsu-ura, H.S., T. Michikawa, K. Suzuki, A.K. and K.M. wrote the manuscript. K.M. supervised the study.

## Additional Information

**Supplementary information** accompanies this paper at <https://doi.org/10.1038/s41598-019-40931-w>.

**Competing Interests:** The authors declare no competing interests.

**Publisher's note:** Springer Nature remains neutral with regard to jurisdictional claims in published maps and institutional affiliations.



**Open Access** This article is licensed under a Creative Commons Attribution 4.0 International License, which permits use, sharing, adaptation, distribution and reproduction in any medium or format, as long as you give appropriate credit to the original author(s) and the source, provide a link to the Creative Commons license, and indicate if changes were made. The images or other third party material in this article are included in the article's Creative Commons license, unless indicated otherwise in a credit line to the material. If material is not included in the article's Creative Commons license and your intended use is not permitted by statutory regulation or exceeds the permitted use, you will need to obtain permission directly from the copyright holder. To view a copy of this license, visit <http://creativecommons.org/licenses/by/4.0/>.

© The Author(s) 2019